Chapter-6
Investigations on tailoring physical properties of RF magnetron sputtered Cadmium Sulphide (CdS) thin films

Chapter 6

6.1 Introduction

Semiconductor nanocrystals have gained great interest in basic and industrial research, due to their outstanding optical and electrical properties. [180, 181, 320] Among the most widely used materials in electronic circuits is cadmium sulfide (CdS). Due to its broad optical band gap in its thermodynamically stable würtzite phase, as well as its chemical and mechanical stabilities, CdS is a nearly ideal semiconductor material for usage in optoelectronics applications. This material is mainly used as a component for numerous applications, such as photo detectors [321], thin-film transistors [322], gas sensors [323], light-emitting diodes [324], and solar cells. [325-328] However, the aggregation of Nano-sized CdS particles has resulted in reduced surface area and a high rate of photo-induced electron-hole recombination. [329-331] Cadmium sulphide (CdS) is a widely used II-VI semiconductor in electro-optics, infrared devices, and mostly as an active element in solar cells such as Cadmium Telluride (CdTe), Copper Indium Diselinide (CIS), Copper Indium Gallium Selenide (CIGS), and more recently in Copper Zinc Tin Sulphide (CZTS). [332]. CdS is an n-type semiconductor that is non-stoichiometric and has a direct optical band gap of 2.42 eV. (bulk CdS). Because CdS's band gap falls in the visible spectral region, it has a significant photo stability in this area.[333]

Studies on CdS thin films have shown their potential in different applications, such as light-emitting diodes, and functional gas sensors. Various thin-film techniques are available for CdS thin film deposition [334-337], including spray pyrolysis [119, 217, 338], molecular beam epitaxy [215, 216], pulsed laser deposition [212], chemical bath deposition [213, 214, 339], sputtering [82, 218, 219], and thermal evaporation. [220, 221] Using a variety of

growth techniques, CdS thin films can be fabricated in various nanostructures like nanobelts [340], nanowires [341, 342], nanorods [343, 344], and nanotubes.

Among the other methods, RF magnetron sputtering can deposit the films at low temperatures with high coverage, better adhesion, and high film quality. RF sputtering is considered to be a relatively slow process among the many processes; however the simplified approach supports in better crystallite alignment and improved grain structure. By withstanding the bombardment of high energy particles species during the subsequent development of transparent conducting layers, sputtering produced CdS performs as an improved passivation layer to the underlying absorber layer. RF sputtering is a simple technique, which permits film deposition very close to thermodynamic equilibrium with minimal loss of material. It is one of the three temperature controlled approaches to grow quality epitaxial thin films with controlled stoichiometric deviation [345]. It also exhibits strong lattice matching with the absorber layer and a simple synthesis process, showing sputtering as a versatile synthesis strategy for CdS. It also increases the excess carrier lifetimes and improves the device's band alignment [346]. The optical bandgap of CdS layer can be improved by thinning the CdS layer by forming alloys at either the cation (CdZnS) or anion (CdS:O) sites. [347] Various reports on the structural, optical, and chemical properties of CdS thin films have been published regarding the variation of oxygen flow rate on deposited films. [348-350]

In this chapter, we have studied the influence of nitrogen (N_2) concentration in Ar/N_2 mixture on the bandgap tunability and structural variations of CdS thin films fabricated by using RF magnetron sputtering. [351] Structural properties revealed that CdS thin film are homogeneous in nature without defects, voids, and have shown a polycrystalline structure

in (002) preferential orientation. Thin films sputtered at a higher concentration of N_2 partial pressure with Ar/N_2 mixture have shown a decrease in optical bandgap by 0.15 eV than those fabricated with pure Ar gas. [352-354] The impact of changing the N_2/Ar sputtering ambient composition on the intrinsic properties of sputtered CdS films are quantified, which can be utilized as an n-type semiconductor layer in second-generation thin-film solar cells, in combination with other absorption layers such as $CuInSe_2$ or CdTe. Therefore, CdS thin films were deposited using RF sputtering technique and studied.

6.1.1 Literature Survey

Sathiya Priya et al. (2018) [355] used a chemical bath deposition approach to deposit Cadmium Sulphide (CdS) thin films. The cubic phase of CdS was discovered by structural investigation. The CdS thin films had a homogeneous surface according to scanning electron micrographs. The presence of Cd and S in the thin films was confirmed by EDAX analysis.

Ameen M Ali et al. (2018) [356] CdS microcrystal which had sphere like morphology was synthesized from the residue obtained after chemical bath deposition. CdS thin films were originally developed as a buffer layer for CdTe solar cells. Thermal evaporation was used to grown CdS thin films on a glass substrate. The CdS thin films were annealed for 40 minutes at 250°C, 350°C, and 420°C. The structural and optical characteristics of CdS thin films were investigated. The films were found to have transmittance ranging from 70% to 90%. The band gap was discovered to be between 2.28 and 2.37 eV.

CdS thin films were produced on ITO substrate at 85°C and 90°C using a chemical bath deposition approach by Fatma Gode et al. (2019). [357] The hexagonal structure of CdS

thin films was found by XRD measurements. The optical band gap was found to be 2.2 eV. The absorber layer was PbS, and the CdS layer was used to fabricate a thin film solar cell. The solar cell in which the CdS film was deposited at 90°C had 4.85 percent efficiency. The solar cell that was used to deposit the CdS film at 85°C had 3.59 percent efficiency. The findings demonstrated that the characteristics of CdS thin films influenced device performance significantly.

Martinez-Landeros et al. (2019) [358] used pulsed laser deposition to deposit CdS thin films at room temperature. To investigate the effect on the development of CdS thin films, the chamber pressure was varied from 0.13 to 1.33 Pa. For various deposition pressures, the CdS thin films displayed hexagonal crystalline structure. The crystallinity of CdS thin films improved as the deposition pressure was increased. When compared to S, Cd had a higher rate of deposition. The CdS films' structural abnormalities were revealed by the broadening of the longitudinal optical Raman peak. The flaws in the crystalline lattice are blamed for the disorder in the CdS thin films, which could be attributable to the species' high kinetic energy during deposition.

Wilson et al. (2020)[359] used chemical bath deposition to create CdS thin films at different temperatures. The samples placed at low temperature revealed a seaweed pattern that crystallized in a cubic structure, whereas the ones deposited at higher temperature showed honey comb-like structures. A rise in bath temperature resulted in an increase in conductivity and photosensitivity. For films deposited at higher temperatures, the photoluminescence intensity was reported in the green band region. When compared to the other samples, the films that had honeycomb-like features performed better.

Isik and his colleagues (2021), [360] This research focuses on the thermal evaporation deposition of CdS thin films. Structure, composition, morphology, and optical properties were explored in depth. Temperature-dependent transmission measurements in the spectral region of 400 to 1050 nm were performed on the materials. The band gap energy was around 2.40 eV. To explore the optical properties of CdS thin films, two different models of light were used to study band gap energy as a function of sample temperature.

CdS thin films were developed by chemical bath deposition technique at varying deposition times by Malihe Maghouli et al. (2019). [361] The development of spherical nanograins was indicated by FESEM pictures. The XRD patterns revealed that all layers were cubic phase, and that the crystallinity decreased as the deposition time rose. The band gap ranged between 2.41 and 2.47 eV. The existence of band tail states in the PL spectra indicated the material's increased electrical conductivity.

Muthusamy et al. (2015) [362] used chemical bath deposition to create CdS thin films on a glass substrate doped with Cu. The crystallinity improved as the doping increased, according to XRD tests. EDX analysis was used to investigate the elemental composition of doped and un-doped CdS thin films. The band gap was discovered to be 2.28 eV. Cu doping of 0.04M in CdS was determined to be optimal. The substitution of Cu into the Cd-S lattice was discovered by PL investigations.

Chemical bath deposition was used to deposit CdS thin films onto ITO substrates by Hong Zhan et al. (2015).[363] To analyze the fluctuation in the CdS thin films, the pH of the solution was varied and annealing was done. The pH was controlled using NH_3H_2O. As the annealing temperature was raised, the intensity and size of the crystallites increased. When

compared to the others, one of the films annealed with $CdCl_2$ displayed a blue shift, which could help improve the efficiency of a solar cell.

6.2. Methods and characterization

6.2.1. Fabrication of film

Cadmium Sulphide (CdS) thin films of different thickness and surface morphology under controlled growth condition with a variation of N_2 concentration have been deposited onto ultrasonically cleaned glass substrates by reactive RF magnetron sputtering (Kurt J. Lesker Co) technique using commercially available CdS powder (99.99% Sigma Aldrich-India). After a conventional cleaning operation using organic solvents, the glass substrates were etched in HCl for 30 seconds. Finally, they were cleaned in de-ionized water for 15 minutes before being dried with N_2 to remove surface contaminants. The sputtered thin films were deposited on the substrate by a locally manufactured and designed RF magnetron sputtering system. It consists of a turbopump and a mechanical pump that provides a base pressure of less than 10^{-7} Torr in a cylindrical chamber. The substrate and the target were separated by a distance of 7 cm. To ensure a uniform layer, a stepper motor was employed to keep the substrates rotating throughout the sputtering operation. The chamber was initially evacuated to a high vacuum of $8x10^{-6}$ Torr. The N_2 concentration was varied from 10% to 30% with a step size of 10 in Ar/N_2 mixture. The gas flow rate of sputtering gas Ar (99.99 percent purity) was set to 60 sccm and deposition time was 60 minutes. All the samples were fabricated with a constant deposition rate.

6.2.2. Characterization

UV-Vis absorption spectrum was studied using Cary 5000 model in the spectral range of 3500 – 2500 nm. SEM micrographs were taken using Energy dispersive spectrometers

Hitachi S4160. The film thickness and optical property were measured using Solver Next, NT-MD. The sheet thickness was measured using PARK systems Atomic force microscope. A monochromatic Al Kα radiation (1486.6 eV) was focused on a sample surface area of 0.7 mm × 0.3 mm. The survey scans were obtained by employing these passing sweeps of 15 eV and a step size of 0.1 eV. The phase identification and chemical compositions of fabricated sputtered films were examined by using XRD, (Stoe XPERT-PRO) with Cu Kα radiation excitation wavelength of 1.541.

Research Methodology

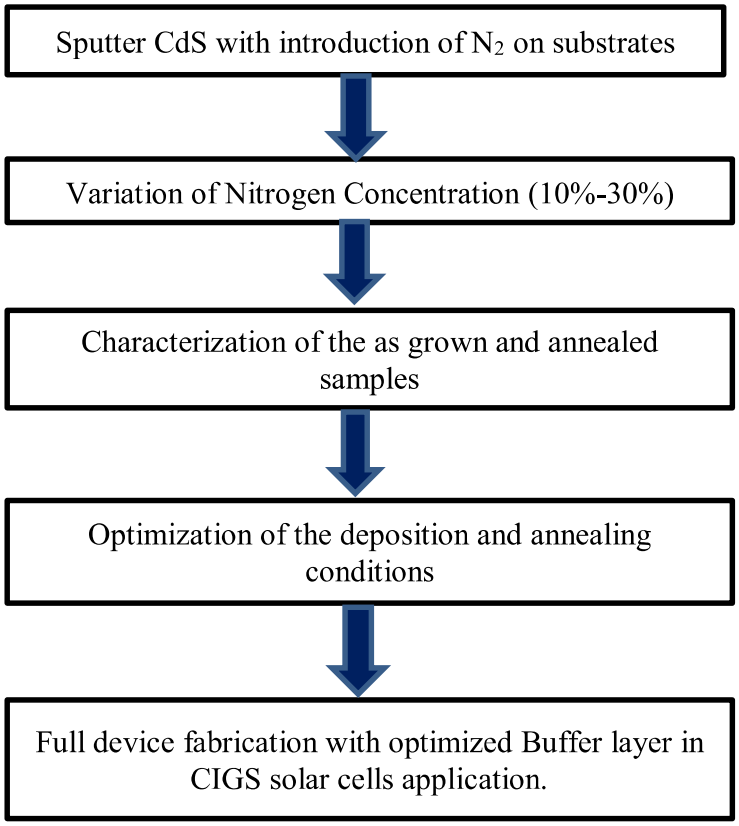

6.3. Results and discussion

6.3.1. Structural studies

The X-ray diffraction plot of the as-deposited and annealed CdS thin film is shown in Figure 6.1 at various nitrogen concentrations. The XRD peak is found to be sharp which indicates that the film is crystalline in nature. A body-centered cubic CdS structure is shown with a preferential growth in the (002) direction. With an increase in N_2 concentration, the strength of significant peaks increases, indicating that crystallization along the corresponding direction is substantially better at higher N_2 concentrations without any changes in orientation preferences. Multiple diffraction peaks are observed at 10% N_2 concentration.

Polycrystallinity is defined as the existence of a significant number of grains in multiple positions throughout a film, resulting in lattice mismatch and misfit. During the deposition process, the micro-strain, which is impacted by the deposition environment or the nucleation of the depositing atoms, can be used to determine the lattice misfit. Dislocation of the atom can also generate a lattice mismatch. [364] Dislocation density and Micro strain, which indicates relative imperfection and the relative misalignment between adjacent crystals, are key considerations. These faulty dislocations are also irregularly distributed across the crystal, unlike defects, imperfections, dislocation, Vacancies in crystals. The following formulas are used to calculate the Micro-strain [365] and Dislocation density [366] of sputtered thin films:

$$\varepsilon = \beta \cos(\theta)/4$$

$$\delta = n/D^2$$

Where β is the full-width half-maximum (FWHM), ε is the strain, and Bragg's angle is θ. D is the average crystallite size, and the lowest dislocation density is n, which is nearly equal to unity.

Scherer's equation was used to calculate the crystallite size [367, 368]-

$$D = 0.9\lambda/\beta \cos\theta$$

Where λ shows the wavelength of the X-ray source (1.5406 Å for Cu-Kα).

Table 6.1 summarizes dislocation density, the grain size, microstrain, and crystallite size for CdS thin films deposited in pure Ar and with different N_2 concentrations in Ar/ N_2 mixture. Due to the higher N_2 flow rate during sputtering, the variation in the mean free path of molecules, the deposited molecules do not have sufficient mobility to settle down in stable orientation.

At higher nitrogen partial pressures, the fluctuation in the mean free route may lead the atoms to alter orientation during the development of thin-film, resulting in a preferred orientation along (002). Furthermore, the reduction in surface energy may be one of the reasons for such an orientation shift. An increment in nitrogen content causes the formation of more vacancies, oxygen interstitials, and causes changes in grain size values. The crystallite size of a sputtered thin film deposited in Ar/N_2 environment is smaller in comparison to the film deposited in pure Ar; implying that the crystallite size of the sputtered film decreases in the presence of N_2. The addition of nitrogen, on the other hand, had no discernible influence on the films' dislocation density or micro-strain.

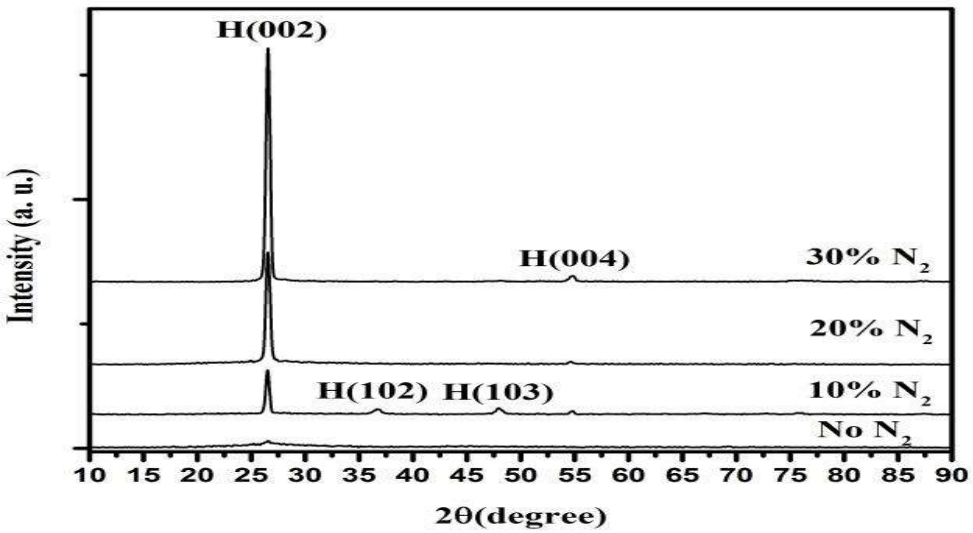

Figure 6.1: XRD pattern of sputtered CdS thin films deposited at different N_2 concentrations in Ar/N_2 mixture.

Table 6.1: Summary of structural parameters of sputtered CdS thin film deposited at various N_2 concentrations in Ar/N_2 mixture.

sample	2θ (002)	β (radian)	D (nm)	$\varepsilon\times10^{-3}$	$\delta\times10^{-3}$ $(nm)^{-2}$
No N_2 (pure Ar)	26.62	0.0201	7.20	21.8	19.2
10% N_2 in Ar/ N_2 mixture	26.56	0.0061	23.43	6.72	1.82
20% N_2 in Ar/ N_2 mixture	26.61	0.0082	17.57	8.94	3.23
30% N_2 **in** Ar/ N_2 mixture	26.61	0.0082	17.57	8.94	3.23

6.3.2. Surface morphology

The field emission scanning electron microscopy (FESEM) images of the as-deposited and sputtered CdS thin films are shown in Figure 6.2 at different nitrogen concentration. The FESEM micrographs show uniform and smooth morphology of the deposited films. The improvement in grain size in post annealed CdS thin films is in good accordance with the XRD results. This proves that sputtering techniques are better when compared to other deposition methods. Smooth uniform film can be seen from the optical microscopy image recorded at 40X magnification as shown in the inset. Figure 6.2 represents FESEM images of films deposited in the pure Ar and with a variation of N_2 concentration in Ar/N_2 mixture. It has been reported that N_2 in films can be present from the residual gas and the working gases (Ar+ N_2). [369-371] The film surfaces exhibit a grassy and rough morphology, as seen in Figures 6.2(a)-6.2(b). The film had a fibrous grain and fine valleys when the N_2 concentration was higher. The rise in N2 concentration promotes a smoother surface, as shown in Figure 6.2(c)-6.2(d). The fibrous grains were developed from the substrate to the surface, resulting in excellent adhesion between the glass substrate and the thick bulk layer. The formation of charge carriers during the reaction with N_2 results in a filled morphology with no voids of spherical grain structures. The density of grain borders decreases as grain sizes increase, and grain boundaries are the principal source of light dissipation within particles. There are essentially no holes in the columnar grains, which are generally generated perpendicular to the substrate in (002) orientation. These properties greatly affect the electrical properties of solar cells when CdS is used as a buffer layer. It has proved that the conversion efficiency of CdS/CdTe solar cells strongly depend on the relatively lesser

roughness of the CdS thin film surface, a reduction in the surface roughness tends to increase the conversion efficiency of these solar cells. [372]

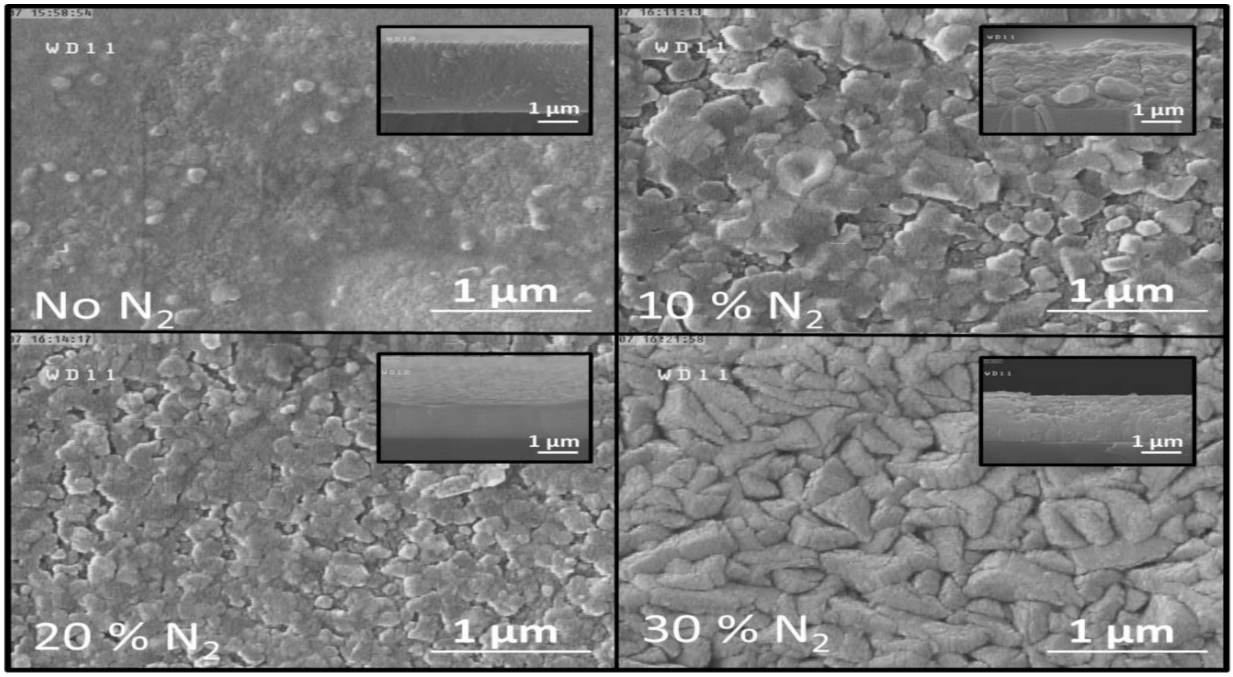

Figure 6.2: FESEM images of sputtered CdS thin films at different N_2 concentrations in Ar/ N_2 mixture.

AFM analysis was utilized to evaluate the surface morphology of CdS thin films at varying N_2 concentrations in Ar/ N_2 mixture. The films are consistent and homogeneous, as evidenced by the AFM images, Figure 6.3. The AFM pictures revealed that the surface is made up of small, tightly packed, and homogeneous structures. The kinetic energy of sputtered CdS particles is lower at lower N_2 concentrations than at higher N_2 concentrations, resulting in more random orientation and various grain sizes, which leads to surface roughness. As the N_2 concentration rises, the kinetic energy of the CdS particles rises and bombardment with high kinetic energy particles can result in increased surface roughness. An increment of kinetic energy at intermediate N_2 Concentration has decreased

the roughness of the surface but increased again at higher N_2 concentration, attributed to the large coarse grain. An incremental rise of N_2 concentration leads to the destruction of the surface and the creation of voids and defects in the structure. Structural properties of CdS thin films deposited with 30% N_2 are remarkably good agreement with the FESEM and XRD spectra.

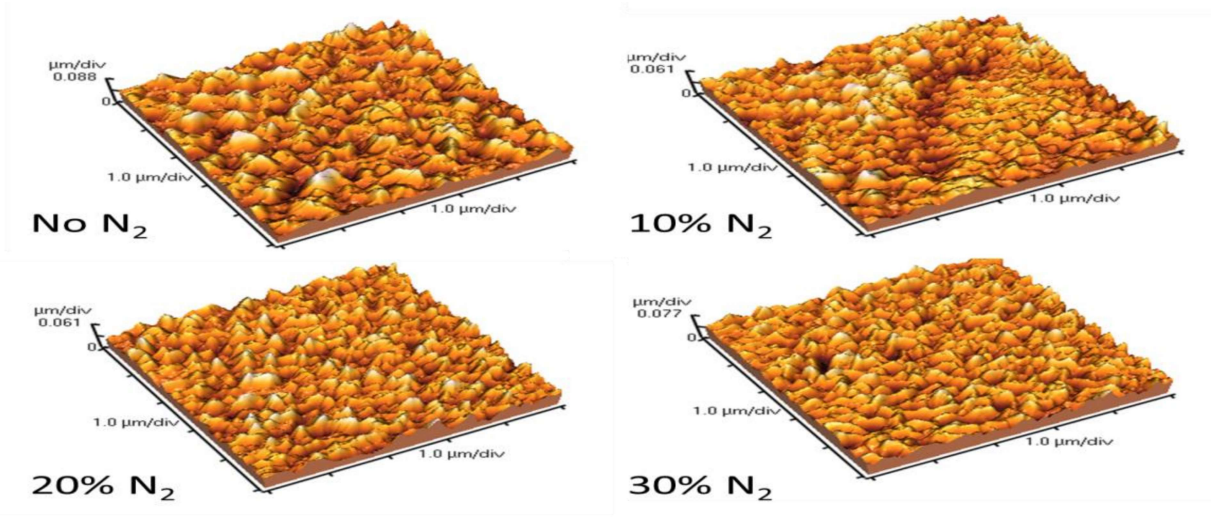

Figure 6.3: AFM images of CdS thin films sputtered at different N_2 concentrations in Ar/ N_2 mixture.

6.3.3. Optical properties

The optical properties of sputtered CdS thin films were evaluated by UV-Vis spectroscopy. The transmittance spectra of CdS thin films at various N_2 concentrations in Ar/ N_2 mixture were measured with the wavelength range 500-2500 nm, as shown in Figure 6.4. Transmission spectra reveal that the average optical transmittance is > 80%, which is appropriate for solar cells and other optoelectronic applications. [373] The structure of the film, which is influenced by different sample preparation techniques, film thickness, and

deposition parameters, has a substantial impact on transmission. The presence of interference fringes in the visible region of transmittance spectra represents that sputtered CdS films have better crystallinity and small defect density near the band edge; whereas the presence of sharp absorption edges in the visible region of transmittance reveals that the films have a smooth surface, supporting the findings from FESEM. [374]

The photo energy bandgap (E_{opt}) and absorption coefficient (α) are related in direct transition semiconductors by [30],

$$\alpha(\mathrm{E})^{1/2} = B(E - \mathrm{Eopt})^{1/2}$$

B represents the optical density of the state, and E is the absorption energy.

The optical band gap energy could be calculated using Tauc's method, $\alpha h\upsilon = \mathrm{A}(h\upsilon - \mathrm{E_g})^{n}$ where α is the absorption coefficient (i.e energy-dependent), h represents the plank constant, hυ is the incident photon energy, A is the absorption edge width parameter, and Eg is the optical band gap energy. The power factor of transition mode is denoted by the constant (n). The values of (n) are 1/2, 2, 3/2, and 3, respectively, and correspond to direct allowed, indirect allowed, direct forbidden, and indirect forbidden transitions. After plotting the photon energy and all of the powerful possibilities of (n) for the sample, the n = 1/2 plot was found to be the most suited. As a result, Tauc's relation will be adjusted. The absorption Coefficient (α) may be estimated using the films' transmittance spectra. Therefore, bandgaps were determined using the modified Tauc's plot equation below-

$$\alpha h\upsilon = \mathrm{A}(h\upsilon - \mathrm{E_g})^{1/2}$$

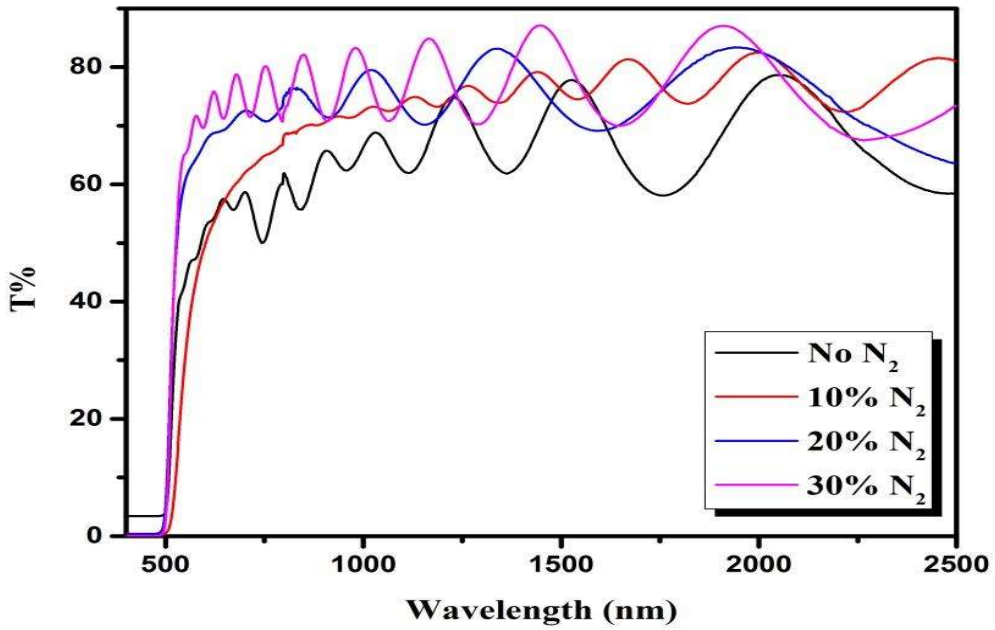

Figure 6.4: Transmission spectra for CdS thin films deposited by sputtering at different N_2 concentrations in Ar/ N_2 mixture.

Figure 6.5 depicts the fluctuation of the optical bandgap as a function of N_2 concentration. The bandgap at pure Ar is about 2.45 eV. When N_2 concentration is increased 10%, 20%, and 30% the band gap reduces from 2.38 eV, 2.35 eV to 2.30 eV, respectively. These band gap values were smaller than the bulk CdS band gap (2.42 eV). [375-377] Our results show that CdS can be an effective window material in different photovoltaic applications such as CdS/CdTe and CdS/Cu_2S solar cells because of its optimized bandgap. [378] The transmittance spectra and energy band diagram of sputtered CdS thin film is shown in Figure 6.4. The thin films show good transparency, exhibiting interference patterns. The optical transmittance spectra of CdS thin film is analysed using the above relation. For suitable value of n, the graph is a straight line and the value of the band gap Eg is obtained

by extrapolating the linear portion of the graph to intercept the photon energy axis [379], which gives the energy gap Eg. Plot for (αhν)2 versus hν for as-deposited CdS thin films is shown in the Figure 6.5. The straight-linenature of the plots show that the transition is direct allowed and the single slope present in the curves suggest that the film is of single phase [219]. The calculated band gap of the CdS thin film is 2.4 eV.

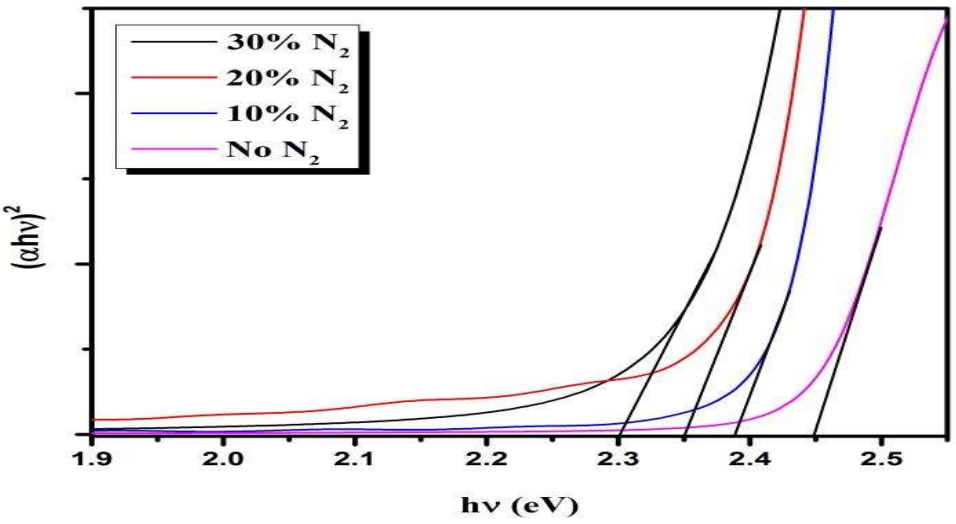

Figure 6.5: Plot of $(\alpha h\upsilon)^2$ vs. photon energy (hυ) for CdS thin films deposited in pure Ar and with the variation of N_2 concentration in Ar/ N_2 mixture.

6.4. Conclusion

To summarize, we investigated the effect of N_2 flow rate on the characteristics of sputtered CdS thin films using RF magnetron sputtering. The structural, optical, and electrical properties of sputtered CdS thin films were studied in relation to the deposition environment, particularly the presence of N_2. The XRD spectrum revealed that increasing the concentration of N_2 in the Ar/N_2 mixture during the deposition of CdS thin films

affected their crystallinity and aggravated their amorphous nature. As the N_2 concentration rises, the crystallinity of the sputtered thin films rises. The surface structural characterization of sputtered thin films are revealed by FESEM and AFM analysis, revealing the formation of continuous, smooth, and dense films free of defects and vacancies such as pinholes, cracks, and protrusion. The bandgap in the Ar/N_2 combination reduces considerably as the N_2 content changes, according to UV-visible absorption spectra. Optical studies demonstrate a considerable increase in transmittance >80 at 500-2500 nm with increased N_2 partial pressure. The optical properties of sputtered CdS thin films can be modified by incorporating N_2 content in Ar gas during the deposition method, according to this investigation. CdS, with its small bandgap (2.30 eV), can be used as a window material in a variety of optoelectronic devices, including solar cells.